

1 Palaeoenvironmental and [palaeoclimatic conditions in the Bhimtal valley, Kumaun Lesser Himalaya](#),  
2 between 40 and 24 ka using granulometric analysis

3  
4 B.S. Kotlia<sup>a\*</sup>, Manmohan Kukreti<sup>a</sup>, Harish Bisht<sup>a</sup>, Biswajit Palar<sup>b</sup>, Martin Seiler<sup>c</sup>, Marie-Josée Nadeau<sup>c</sup>, A.  
5 K. Singh<sup>d</sup>, L. M. Joshi<sup>e</sup>, Anupam Sharma<sup>f</sup>, Rajkumar Kashyap<sup>g</sup>, Pooja Chand<sup>a</sup>, Kalpana Gururani<sup>a</sup>,  
6 Abhishek Mehra<sup>a</sup>

7  
8 <sup>a</sup>Centre of Advanced Study in Geology, Kumaun University, Nainital, 263001, India

9 <sup>b</sup>Centre for Ocean, River, Atmosphere and Land Sciences, Indian Institute of Technology, Kharagpur,  
10 721302, India

11 <sup>c</sup>The National Laboratory for Age Determination, Norwegian University of Science and Technology,  
12 NTNU University Museum, Trondheim, Norway

13 <sup>d</sup>Centre of Advanced Study in Geology, University of Lucknow, 226007, India

14 <sup>e</sup>Government Inter College, Tilsari Garur, Bageshwar, Uttarakhand, 263641, India

15 <sup>f</sup>Birbal Sahni Institute of Palaeosciences, 53 University Road, Lucknow, 226007, India

16 <sup>g</sup>Indian Institute of Technology, Roorkee, 247667, India

17  
18 \*Corresponding author: [bahadur.kotlia@gmail.com](mailto:bahadur.kotlia@gmail.com) (B. S. Kotlia)

19  
20 **Abstract**

21  
22 [In this research, we conducted a detailed granulometric analysis of 9.5 m thick palaeolake succession,](#)  
23 [exposed at Bilaspur \(Bhimtal\) in the Kumaun Lesser Himalaya to reconstruct the palaeoenvironmental](#)  
24 [and palaeoclimatic conditions. We carried out statistical parameters of grain-size data \(i.e., standard](#)  
25 [deviation, kurtosis, and skewness, bivariate plots\), and end member modeling analysis \(EMMA\) and our](#)  
26 [study reveals sediment's unimodal and bimodal nature, deposited via fluvial action under low to high](#)  
27 [energy environmental conditions since the origin of the lake. Some parts of the deposit show poorly](#)  
28 [sorted and mixed character \(leptokurtic to platykurtic\) of sediments, indicating that the sediments were](#)  
29 [primarily transported from the proximal area of the lake basin under low-energy environmental](#)  
30 [conditions. The finely skewed and poorly sorted sediments show different modes of grain size](#)  
31 [distribution, which are attributed to fluctuations in the hydrodynamic conditions of the lake. The arid](#)  
32 [climatic conditions prevailed in the valley from ca. 42-40 ka BP, followed by warm and moist conditions](#)  
33 [from ca. 40-39 ka BP. The arid conditions under the low rainfall regime were experienced by the valley](#)  
34 [from ca. 39-30 ka BP, while it exercised another episode of moist and warmer conditions from ca. 30-24](#)  
35 [ka BP. Further, the end-Member Modeling Analysis \(EMMA\) shows four end members \(EM1-EM4\) with](#)  
36 [different climatic conditions during the deposition, e.g., clay to fine silt-size particles reflecting higher](#)  
37 [lake levels under warm-wet climatic conditions, coarse silt fraction representing moderate energy](#)  
38 [conditions, and fine to coarse sand fractions indicating shallow lake-level conditions in the arid climatic](#)

39 conditions as well higher energy flow. The interpretation of energy conditions in the lake and catchment  
40 area by using various methods reveal different palaeoenvironmental conditions during the sediment  
41 deposition.

42

43 Keywords: Kumaun Lesser Himalaya; Palaeolake deposits; Granulometric analysis; Statistical  
44 parameters; End Member Modeling Analysis (EMMA)

45

## 46 **1. Introduction**

47

48 Lakes are valuable source of continuous sedimentary archives as well as complex systems that can offer  
49 diverse physical, chemical, and biological data (Adrian et al., 2009) which can be utilized as a proxy to  
50 quantify the response of the ecosystem, earth surface processes, and anthropogenic influences on the lake.  
51 As the internal feedback mechanism of lakes is governed by various factors such as catchment size,  
52 geology, climate, morphometry, land use and land cover in the surrounding area, it is essential to consider  
53 parameters like sedimentation rate, organic productivity, lake bottom sediment texture and bathymetry to  
54 understand the dynamics of the lake (Flemming, 2007). Among the different natural records, such as  
55 deep-sea sediments, loess, ice cores, coral, peat, varves and tree rings etc., the lacustrine material stands  
56 out a large geographic distribution, extensive long time span with excellent continuous records of layering  
57 of sedimentations and a wealth of environmental data. As a result, it plays a crucial function as a primary  
58 indicator for understanding global climate changes over a range of different time intervals (Chen et al.,  
59 2004). Sediment deposition in lakes is often continuous, offering valuable insights into significant  
60 climatic fluctuations in the past (Kotlia et al., 2023). The Himalayan lakes are sensitive indicators of  
61 climatic as well as environmental changes with implications at both regional and global levels. These  
62 serve as important archives for palaeoclimatic studies, storing valuable information about climatic history.

63 A granulometric analysis is an essential sedimentological tool to interpret the depositional environment  
64 and hydrodynamic conditions. The sizes of particles are intricately connected to factors such as  
65 turbulence, wave energy and proximity to the shoreline, sediment transport processes, energy levels and  
66 erosional strength, as coarsening or fining of the particles can signify intensified or weakening erosion  
67 strength (Wang et al., 2016). Generally, larger grain sizes are associated with higher energy conditions  
68 during sediment production or transport, while smaller grain sizes suggest lower energy levels. These  
69 changes in particle size reflect the dynamics of erosion processes occurring within the lake and its  
70 surrounding catchment area. During periods of higher lake levels, finer sediment particles tend to be  
71 deposited in the central part of the lake, while coarser particles are typically confined to the near shore

72 zone (Rawat et al., 2021). Conversely, the lake's center would be relatively closer under lower lake-level  
73 conditions, and coarser particles would be deposited under high-energy conditions (Bird et al., 2014;  
74 Rawat et al., 2021). Thus, variations in grain size within the sediment over time, particularly an increase  
75 in the presence of sand, can indicate periods of drier and warmer climates, corresponding to lower lake  
76 levels. Conversely, a decrease in sand content may indicate periods of wetter and colder climates (Alin  
77 and Cohen, 2003).

78 The Grain Size Distribution (GSD) data are primarily generated datasets frequently utilized for  
79 sedimentology and other Earth science studies. The end-members are defined as the numerical separation  
80 of GSD data into its parts, which provide information on palaeoenvironmental conditions (Weltje and  
81 Prins, 2003; Meyer et al., 2013) and also help to understand the sedimentary provenance and depositional  
82 regimes/processes (Paterson and Heslop, 2015). Regarding statistics, the concept of end members is more  
83 reliable in describing the depositional habitats. The overall values of end-member modeling analysis  
84 (EMMA) have already been extensively documented by Weltje and Prins (2003, 2007). This modeling is  
85 an excellent application and functional tool which can eliminate GSDs into geologically relevant sections,  
86 estimate end members and be regarded as a nonparametric technique (Paterson and Heslop, 2015).

87

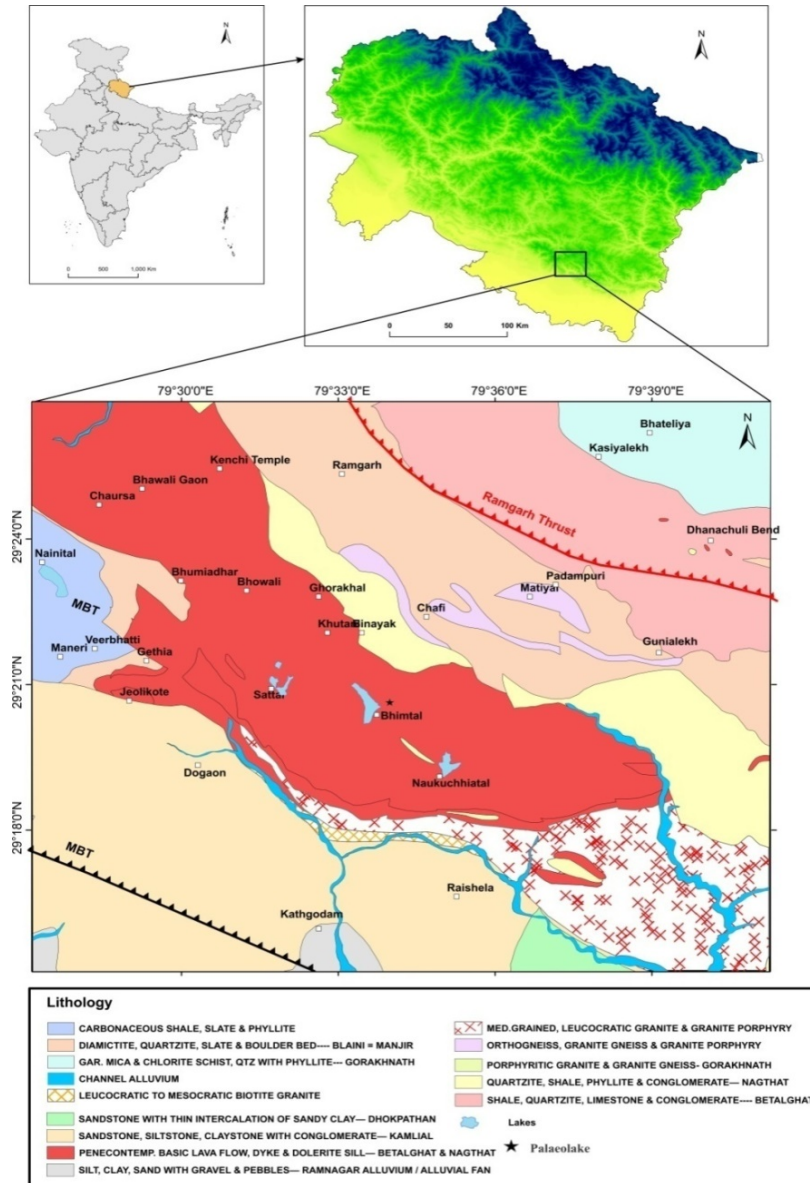
## 88 **2. Study area and regional geology**

89

90 The Bhimtal region (79°30' to 79°36' E: 29°19' to 29°24' N), covering a part of Survey of India (SOI)  
91 Toposheet No. 53 O/11, lies in the Kumaun Lesser Himalaya. The landscape is rough, including large  
92 valleys, low and high hills, escarpments, gorges and rivers. The NW-SE extended median part creates a  
93 vast step-like valley with numerous lakes and separating terrace-like plains. The steep hills with quartzite  
94 caps and trapean rocks beneath them are located east and west of this chain of lakes. These ridges on  
95 either side of the diagonal valley represent the two flanks of an asymmetrical anticline.

96

97 The Kumaun region of the Lesser Himalaya is home to several lakes, including Bhimtal, Naukuchiatal,  
98 and others, which are connected to the active Main Boundary Thrust (MBT) in the south and the Ramgarh  
99 Thrust in the north. The Ramgarh Thrust (RT) in the north and the Main Boundary Thrust (MBT) in the  
100 south (see Fig. 1) are sandwiched by the Lesser Himalayan sequence which exhibits numerous periods of  
101 deformation. The Bhimtal area is made up of the rock of Bhimtal Volcanic formation, which is made of  
102 basalt, and is stratigraphically exposed beneath the Bhowali Quartzite (Nagthat Formation), Jantwalgaon



103  
104 Fig. 1. Geological map around the study area

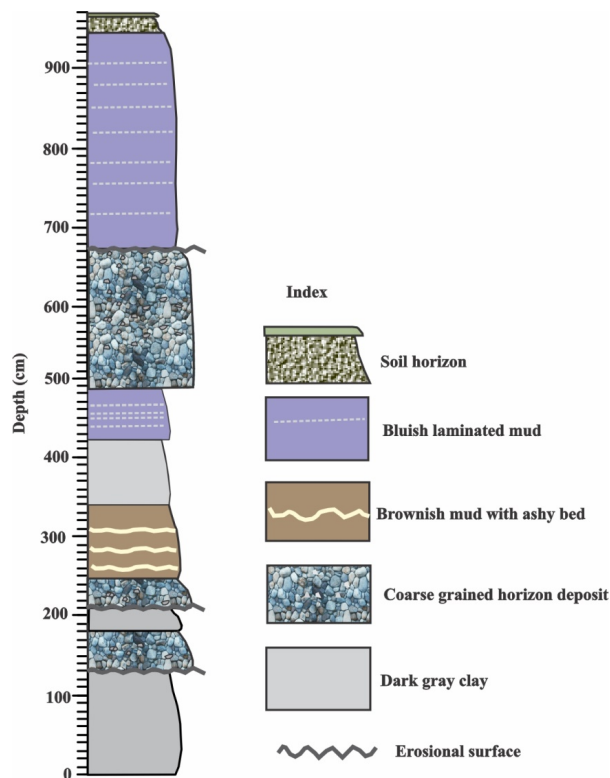
105  
106 and interspersed there in are shale horizons (Valdiya, 1988; Kotlia et al., 1997; Pant and Shukla, 1998)  
107 (Fig.1). Presence of a series of depressions linking Bhimtal and Naukuchhiatal suggests that these lakes  
108 were originally a single large lake (Khanka and Jalal, 1985; Kotlia, 1995). The ancient lake that occupied  
109 this low-lying area was likely 7-10 km long and 1 km wide. Further evidence of the lake's existence can  
110 be found in the alluvial and lacustrine deposits along the WNW-ESE trending Nagari-Naukuchhiatal  
111 valley. Such lakes, formed during the Quaternary period have been described throughout the Himalaya  
112 (Kotlia, 1992; Kotlia and Rawat, 2004; Kotlia and Joshi, 2013; Kotlia et al., 1997, 1998, 2000, 2010,  
113 2023; Valdiya et al., 1996; Kothiyari et al., 2020).

114 **3. Field measurements and lithostratigraphy**

115

116 The exposed sequence consists of approximately 9.5 m sediment, including mud, unconsolidated sands,  
117 silty clays and gravel (Fig. 2). The sequence begins with dark grey clay (0-130cm), representing perhaps  
118 the moderate energy conditions. Upward from 130-180 cm, the section comprises coarse grained material,  
119 followed by dark grey clay from 180-210 cm and further followed by a coarse grained horizon from 210-  
120 250 cm. From 250-340 cm, brownish mud with cm scale ashy beds is present, followed by dark grey clay  
121 from 340-440 cm. From 440-480 cm, the profile comprises bluish colored laminated mud, followed by  
122 coarse grained clay and mud from 480-670 cm. The bluish laminated mud is dominant from 670-948 cm,  
123 and soil horizon is exposed on the top. A systematic sampling was conducted at 5 cm interval for  
124 comprehensive sedimentological investigations.

125



126

127 Fig. 2: Lithology of Bhimtal palaeolake profile

128

129 **4. Chronology**

130

131 Four AMS radiocarbon dates were obtained from the Bhimtal palaeolake profile. The AMS radiocarbon  
132 dating was performed at NTNU University Museum, Norway. An additional radiocarbon age from the

133 Kotlia et al. (1997) was also used for the same profile. The sediment samples were carefully examined  
 134 under a high-power microscope to remove any micro roots, threads, plastic or other contaminants that  
 135 could affect the accuracy of the dates. After eliminating the unnecessary material, the samples underwent  
 136 Acid-Base-Acid Test (ABA). Subsequently, the samples were freeze-dried for 12 hours, and the dried  
 137 samples (2mg) were packed into tin foil capsules. These capsules filled with samples were placed in  
 138 an auto-sampler for the graphitization process, and the samples were then subjected to  $^{14}\text{C}$  AMS dating  
 139 using an AMS instrument.

140  
 141 The Age-depth modeling of the obtained radiocarbon ages was performed using OxCal software (version  
 142 4.4.4) (Bronk Ramsey 2009), employing the P\_Sequence age-depth model with a variable deposition rate  
 143 parameter, k (Bronk Ramsey and Lee, 2013). The uncorrected AMS  $^{14}\text{C}$  dates were calibrated into years  
 144 before present (cal yr BP), specifically 1950 AD. The terrestrial calibration curve IntCal20 was utilized  
 145 for calibration (Reimer et al., 2020). The calibrated ages ranged from 41,877 cal yr BP (at a depth of 0  
 146 cm) to 25,776 cal yr BP (at a depth of 850 cm). The details of the obtained ages are presented in Table 1.  
 147 The age of the individual zone of the palaeolake was extrapolated with the help of OxCal age depth  
 148 model. The modeled ages at 95% confidence interval ( $2\sigma$ ) are shown in Fig. 3.

Lab. no.	Sample depth (cm)	$^{14}\text{C}$ date ( $^{14}\text{C}$ yr BP)	Calibrated age range (cal yr BP)	Calibrated median age (cal yr BP)
TRa-16468	0	37,337±961	42,944-40,605	41,877
TRa-16471	210	33,499±859	40,232-36,906	38,587
TRa-16474	445	31,185±286	36,074-34761	35,470
TRa-16475	485	27,341±205	31,734-31,107	31,401
RCa	850	21,500±1300	28,352-23,144	25,776

155  
 156 Table 1.  $^{14}\text{C}$  dates obtained on bulk sediments from the Bhimtal palaeolake profile  
 157

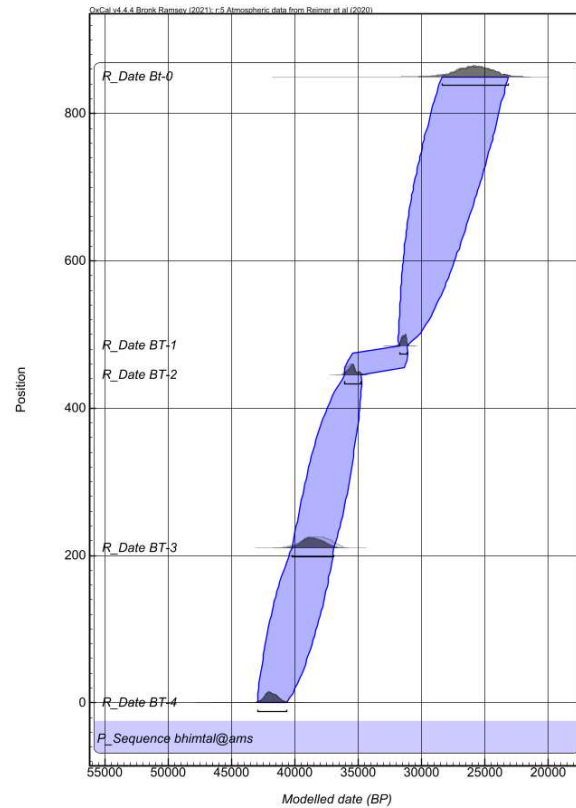
## 158 5. Granulometric analysis

159  
 160 A total of 77 samples were collected for grain size analysis. The standard method for grain size analysis  
 161 was followed by Kotlia et al. (2023). The samples were dried at 50°C in a hot air oven. Each sample (2  
 162 gm) was added to a centrifuge tube containing 10 ml of Sodium Acetate. The tube was heated for one  
 163 hour, and this process was repeated twice for each sample. After centrifugation, 2 ml of  $\text{H}_2\text{O}_2$  was added  
 164 to the sample, followed by boiling for one hour. The sample was then left in a tube overnight. The next  
 165 day, the samples underwent centrifugation and decanting twice. Subsequently, the samples were treated  
 166 with Sodium Bicarbonate (10 ml), Sodium Citrate (0.2 ml), and Sodium Dithynide (0.2 gm) and boiled

167 for one hour. After three rounds of centrifugation and decanting, the chemically treated samples were  
168 ready for further analysis.

169

170 The granulometric analysis of the chemically treated samples was performed using a Laser Particle Size  
171 Analyzer (LPSA). The data obtained from the analysis was processed using Gradistat software (Blott and



172

173 [Fig. 3. Age depth plot for Bhimtal palaeolake profile using OxCal.](#)

174

175 Pye, 2001) to conduct further granulometric analysis.

176

## 177 **6. End-Member Modelling Analysis (EMMA)**

178

179 The MATLAB GUI package AnalySize provides complete capabilities for analyzing the GSD data. It  
180 processes various data formats obtained from the Particle Size Analyzers instrument (Paterson and  
181 Heslop, 2015). The AnalySize can save a fitting session to a standard MATLAB data file to save time  
182 when examining massive data sets. It is easy user interface for loading the data files and transferring the  
183 results to others. In order to distinguish between the various subpopulations within the sediment grain size  
184 components, the preferred number of end members was chosen.

185 **7. Results and discussion**

186

187 **7.1. Grain size statistics**

188

189 Based on the grain size distribution, sediment color variations and lithofacies, the profile has been divided  
190 into nine zones which are labeled as Zone-I to Zone-XI (Fig. 4). This division allows for a more  
191 comprehensive examination of the sediment characteristics and their variations.

192

193 Zone-I (0-30 cm; 41,877-41,460 cal. yr BP). The grain size ranges between 3.7-6.1  $\phi$  (average 5.4 $\phi$ ),  
194 indicating a composition of medium silt to very fine sand. The silt, sand and clay components are present  
195 as 70.2%, 22.5% and 7.6% respectively. The sand percentage ranges from 9.9% to 56.2%, the silt from  
196 39.5% to 81.7%, and the clay from 4.3% to 9.3% (Fig. 4). The high sandy silt concentration indicates  
197 high-energy depositional environment and suggests low rainfall situation in the catchment (e.g., Warriar  
198 et al., 2013). The sediment types in Zone-I vary from unimodal to bimodal, and its texture is classified as  
199 sandy mud.

200

201 Zone-II (30-110 cm; 41,460- 40,170 cal. yr BP). The grain size varies from 4.7-6.6 $\phi$  (average 5.7 $\phi$ ),  
202 indicating medium silt to coarse silt. The sediment comprises an average value of sand as 18.0%, silt as  
203 73.7% and clay as 8.3% with silt being the significant component. The content of sand varies between  
204 5.6-39.5%, while the silt and clay concentrations range between 55.8-83.1% and 4.7-12.9%, respectively  
205 (Fig. 4). The highest sandy silt concentration indicates high-energy environmental condition during the  
206 sediment deposition. It also reveals lower rainfall in Zone-II as compared to Zone-I. The sample types  
207 vary between unimodal and bimodal in nature, and their texture is classified as mud to sandy mud.

208

209 Zone-III (110-190 cm; 40,170-38,890 cal. yr BP). The size of the grain varies from 4.3-6.9 $\phi$  (average  
210 5.6 $\phi$ ). The dominant components are silt (66.0%), followed by sand (18.0%) and clay (7.4%). The sand  
211 percentage varies between 3.9-55.3%, the silt ranges from 41.1-84.7% and the clay ranges from 3.6-  
212 11.4% (Fig. 4). The silt concentration in this zone is the highest, suggesting high precipitation and low-  
213 energy environmental condition. The sample type in Zone-III is unimodal and bimodal, with a texture of  
214 sandy mud to muddy sand in nature.

215

216 Zone-IV (190-290 cm; 38,890-37,460 cal. yr BP). The grain size distribution ranges from 4.4 to 6.4 $\phi$   
217 (average 5.6 $\phi$ ), showing a concentration of silt from medium to very coarse in size. The sediment  
218 comprises sand as 22.1%, silt as 74.9%, and clay as 6.7%, with silt being the primary constituent,



219 followed by sandy clay. The percentage of sand varies between 3.8 to 41.9%, while silt and clay are  
220 present in relatively minor amounts, ranging from 55.6 to 85.7% and 2.5 to 10.5%, respectively (Fig. 4).  
221 The high sandy silt concentration suggests a high-energy environmental condition and indicates less  
222 precipitation or dry conditions in the catchment. The sample type is unimodal and bimodal in this zone,  
223 with a sandy mud-to-mud texture.

224  
225 Zone-V (290-440 cm; 37,460-35,510 cal. yr BP). The mean size of grain ranges between 4.6-6.5  $\phi$   
226 (average 5.4 $\phi$ ), indicating medium silt and very coarse silt. The sediment consists of an average of 26.3%  
227 sand, 66.8% silt and 6.8% clay, with silt being the significant constituent, followed by sand and clay.  
228 Sand percentages vary between 5.0-43.6%, while silt (51.3-85.3%) and clay (3.8-10.3%) also vary (Fig.  
229 4). The high sandy silt concentration suggests that the sediment was deposited under the high-energy  
230 depositional conditions, which may be coupled with low precipitation or dry climatic conditions. The  
231 sample types in Zone-V are unimodal, bimodal and polymodal, with a texture of sandy mud to mud.

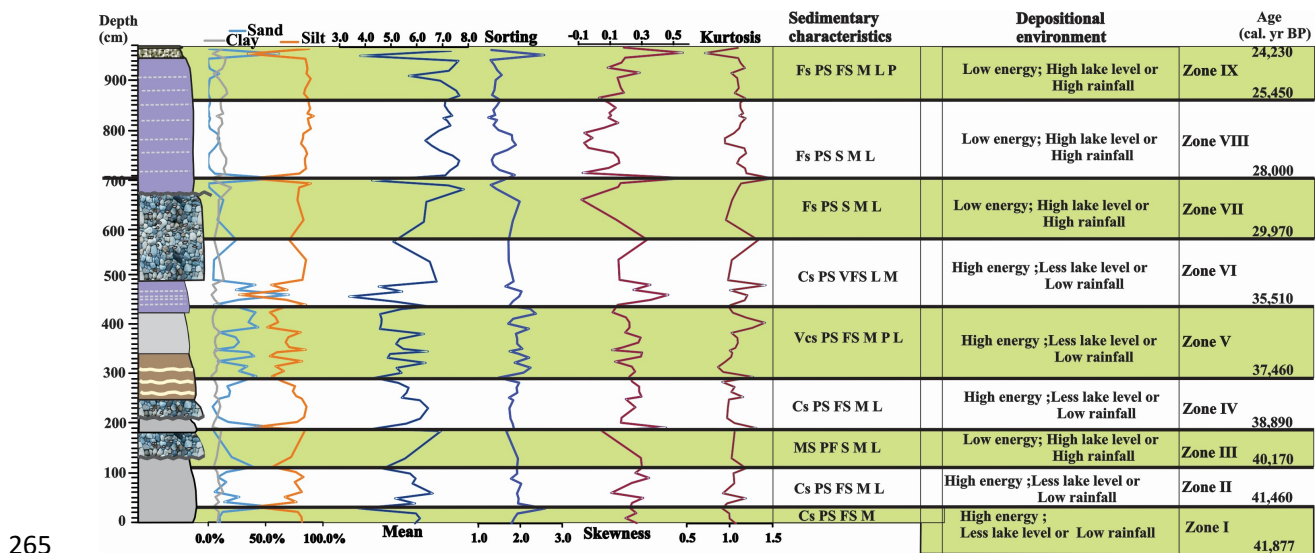
232  
233 Zone-VI (440-590 cm; 35,510-29,970 cal. yr BP). It is characterized by an average grain size ranging  
234 from 3.4-6.8 $\phi$  (average 5.3 $\phi$ ), indicating medium silt to very fine sand. The composition is characterized  
235 by silt as a significant constituent, followed by sand and clay, with average sand (28.0%), silt (65.2%) and  
236 clay (6.8%). The sand concentration varies widely from 4.3-70.2%, while the silt (26.9-70.5%) and clay  
237 (2.9-13.5%) contents are relatively consistent (Fig. 4). The high sandy silt concentration suggests a  
238 depositional environment with high energy and low rainfall or dry climatic conditions. Zone-VI ranges  
239 from unimodal to bimodal and belongs to the texture of sandy mud to mud in nature.

240  
241 Zone-VII (590-710 cm; 29,970-28,000 cal. yr BP). The size of the grain varies between 4.3-7.8 $\phi$  (average  
242 6.6 $\phi$ ) with a composition of very coarse silt to fine silt. The mean values of silt, sand, and clay contents  
243 are 75.8%, 12.9%, and 11.3%, respectively, with silt as the primary constituent, followed by sand and  
244 clay content. The concentration of sand has a range from 0.0-60.9%, while silt (36.6-89.5%) and clay  
245 (2.5-19.9%) are also present (Fig. 4). The high silt concentration suggests that the sediment was deposited  
246 under low energy conditions and moist climatic conditions. The sample types in Zone-VII are unimodal,  
247 bimodal and trimodal, with a texture of sandy mud to mud.

248  
249 Zone-VIII (710-870 cm; 28,000-25,450 cal. yr BP). This zone is characterized by grains ranging from  
250 6.3-7.6 $\phi$  (average 7.1 $\phi$ ) with medium to fine silt. The composition consists of 2.3% sand, 85.9% silt, and  
251 11.8% clay, with silt as the primary component, followed by sand and clay. The sand concentration  
252 fluctuates between 0.0-9.6%, while silt (81.0-92.0%) and clay (7.4-16.5%) also fluctuate (Fig. 4). The

253 highest silt concentration reflects a low-energy environmental condition related to high precipitation or  
 254 wetter climatic situations. The sample types in Zone-VIII are unimodal, bimodal, and trimodal with a  
 255 texture of mud.

256  
 257 Zone-IX (870-948 cm; 25,450-24,230 cal. yr BP). It has a mean grain size between 3.5-7.6 $\phi$  (average  
 258 6.6 $\phi$ ) and is composed of fine silt to very fine sand. Silt is the significant component, with an average  
 259 concentration of 79.2%, followed by sand as 10.6% and clay as 10.2%. The sand concentration fluctuates  
 260 between 0.0-61.7%, while the silt and clay concentrations range from 34.5-89.4% and 3.9-15.3%,  
 261 respectively (Fig. 4).The high concentration of silt suggests low-energy depositional environment  
 262 characterized by high rainfall and wet climatic conditions during deposition. The sediment samples  
 263 exhibit unimodal to bimodal distribution. The textural group of the sediment ranges from mud to muddy  
 264 sand, indicating a mixture of fine particles (mud) and coarser particles (muddy sand).



265  
 266 Fig. 4: Bhimtal palaeolake sediments exhibiting variations in composition of sand, silt, and clay, expressed as  
 267 percentages. The sediments display mean grain size, sorting, skewness, kurtosis, sedimentary characteristics and the  
 268 environment of deposition. Vcs= very coarse silt, Ms= medium silt, Cs= coarse silt, PS= poorly sorted, FS= fine  
 269 skewed, S= symmetrical, M= mesokurtic, L= leptokurtic, P= platykurtic.

270  
 271 Our data on concentration of grain size indicate that the deposition of the Bhimtal lake sediments  
 272 predominantly occurred in high-energy environmental regime. Zones I, II, IV, V and VI specifically  
 273 experienced high-energy conditions, under arid environment. As a result, the lake area would have  
 274 contracted, and the shoreline would have moved closer to the lake's center. This proximity to the  
 275 shoreline led to the deposition of coarser sediments (e.g., Finney and Johnson, 1991; Shuman et al.,  
 276 2001). On the other hand, zones III, VII, VIII and IX exhibit low-energy conditions, indicating high lake  
 277 level during sediment deposition due to increased precipitation. In this climate, the lake level would have

278 risen and expanded, allowing for the deposition of fine particles. The coarser particles, however, would  
279 have been deposited closer to the lake shore (e.g., Menking, 1997; Chen and Wan, 1999).

280

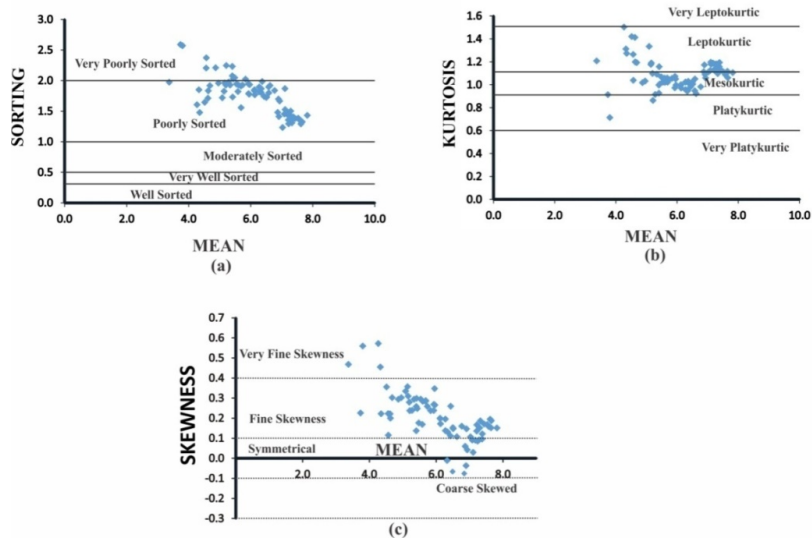
## 281 7.2. Bivariate plots

282

283 Bivariate plots are used to examine the relationship between two variables and can be used to understand  
284 the relationship between grain size and other sediment characteristics, such as energy conditions,  
285 depositional settings, hydrodynamic conditions and deposition agents. These plots can provide essential  
286 insights into the processes that led to sediment formation and help interpret depositional environments.

287

288 **Relationship between Mean size ( $M_z$ ) versus sorting.** The mean vs. standard deviation plot (Fig. 5a)  
289 illustrates that the sediments are distributed across a region, indicating poor sorting. This distribution  
290 suggests that a majority of the samples exhibit low levels of sorting. As the mean grain size transitions  
291 from sand to silt, the level of sorting decreases. Poorly sorted sediments indicate that they were deposited  
292 in a low-energy environment (Blot and Pye, 2001; Padhi et al., 2017; Kotlia et al., 2023).



293

294 Fig. 5. Bivariate plots. (a) mean vs. sorting, (b) mean vs. kurtosis, (c) mean vs. skewness

295

296 **Relationship between Mean size ( $M_z$ ) and Kurtosis ( $KG$ ).** Based on the bivariate plot of mean size and  
297 kurtosis (Fig. 5b), most sediments exhibit a mesokurtic nature with kurtosis values ranging from 0.9 to  
298 1.1. The mean size varies from very fine sand to medium silt, exhibiting a highly mesokurtic distribution.  
299 In contrast, the remaining section, consisting primarily of silt, exhibits distributions ranging from  
300 leptokurtic to platykurtic. The sand units specifically demonstrate a platykurtic distribution.

301 **Relationship between Mean size ( $M_z$ ) and Skewness ( $SK$ ).** Based on the bivariate plot of mean size and  
 302 skewness (Fig. 5c), it can be observed that the skewness values exhibit a range from very fine to  
 303 symmetrical. The very fine skewed values ranged from 0.2 to 1.2, the fine skewed values from 0.3 to 0.1,  
 304 very fine skewed values from 0.3 to 0.6, and symmetrical skewed values fell between -0.1 and 0.1. The  
 305 grouping of sediments within the fine-skewed zone, as depicted in Fig. 5c, suggests the presence of finely  
 306 skewed sediments. This skewness is a result of inclusion of silt particles into the sand component.

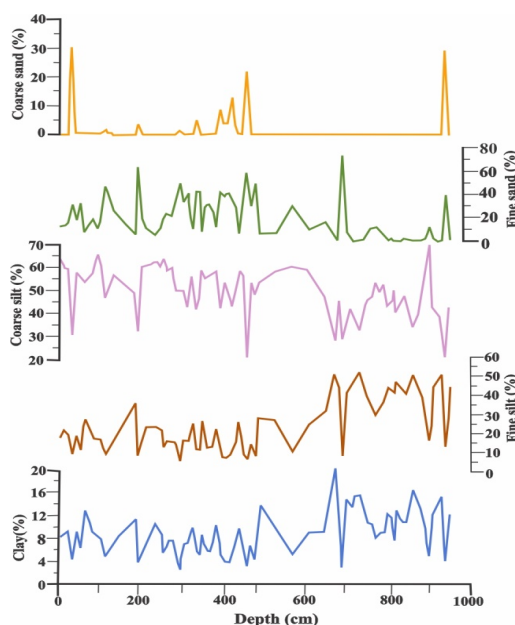
307

### 308 7.3. End Member Modeling Analysis (EMMA)

309

310 The EEMA of Bhimtal sediment profile was carried out to understand the end-members (EM) that help to  
 311 understand the sedimentation process by analyzing different grain-size parameters, distribution and the  
 312

312



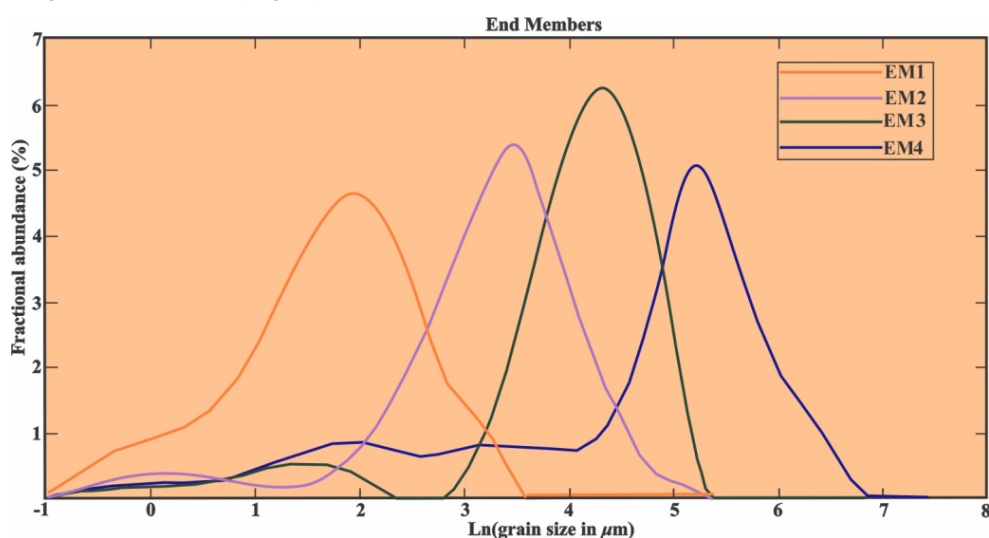
313

314 Fig. 6. Grain size variation with depth for Bhimtal lake profile

315

316 different modes of end-members. The grain size data depicts ranges in clay from ~2.5 to 20%  
 317 (average=8.90%), silt ~27–92% (average = 74.50%) and fine sand fractions of ~0-70% (average=  
 318 16.60%) (Fig. 6). The EM1 exhibits a dominant mode peak at around 2  $\phi$  (very fine silt and clay). It  
 319 varies from 0 to 100% (average = 47%). The EM2 exhibits a symmetrical unimodal peak in the very  
 320 coarse silt range (mode at 3.5  $\phi$ ) with proportions ranging from 0-77% (average = 35%). The EM3 is  
 321 characterized by asymmetrical unimodal peak centered a around 4.4  $\phi$  (fine sand) from 0–92% (average =  
 322 13%), and EM4 exhibits a bimodal structure with a dominant mode at around 5.3  $\phi$  (coarse sand) from 0–

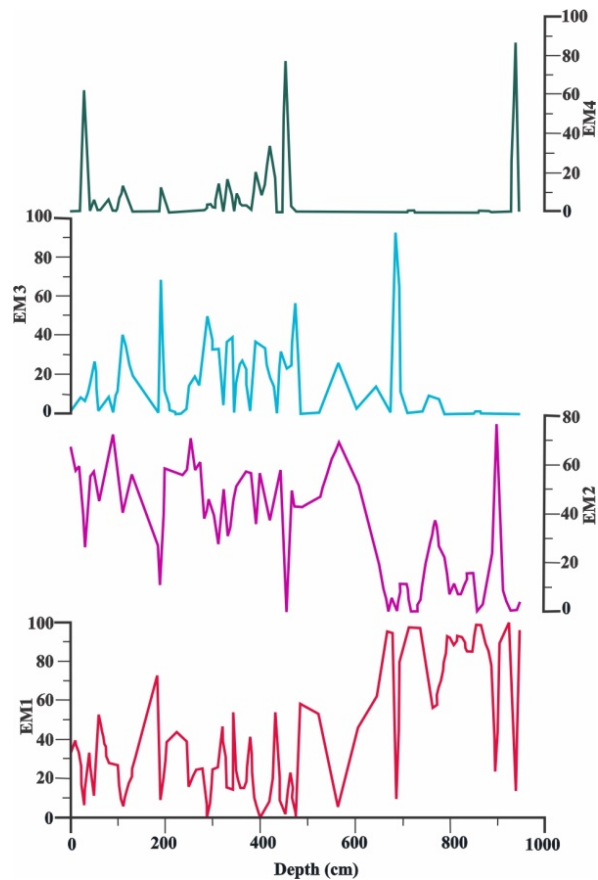
323 87% with an average of 6%. The EM4 also shows additional minor modes. The EM1 has an average  
 324 fractional abundance of 4.6, which is dominant in bluish-color laminated mud rich in clay and fine silt for  
 325 the lithologic unit. The EM2 exhibits high coarse silt and clay representing brownish mud with an ashy  
 326 bed and relatively high in dark grey silty clay and landslide materials (average 5.4). The third end-  
 327 member (EM3) displays relatively low values in bluish laminated mud and comparatively high values in  
 328 dark grey clay and brownish mud (average of 6.3). EM4 is only recorded in a few layers of dark grey clay  
 329 with an average value of 5.10 (Fig. 7).



330  
 331 Fig. 7. Energy model diagram of Bhimtal profile showing variation with different energy conditions (EM1 – EM4)  
 332 with depth  
 333

334 The end members (EM) help to identify transportation processes and sediment flux to the lake for model  
 335 analysis. Four end members (EM1, EM2, EM3 and EM4) extracted from energy modeling reflect the  
 336 lake's energy conditions as shown in the Fig. 8. The EM1 shows the clay to fine silt-sized fraction, which  
 337 deliberates less water supply into the lake and corresponds to higher lake levels under warm-wet climatic  
 338 conditions. The EM2 is indicated by the more significant deposition of coarse silt fraction components,  
 339 reflecting a very shallow lake environment in moderate energy conditions. The EM3 and EM4 represent  
 340 fine to coarse sand fractions during shallow lake-level conditions, possibly under drier climatic conditions  
 341 with higher energy flow. The EM3 is opposite to EM2 from 0-500 cm and shows similar trends with EM1  
 342 from 500-700 cm depth (Fig.8). The energy model of the lake provides the changes in the hydrological  
 343 energy conditions of the catchment area and the transportation medium. These conditions help to interpret  
 344 the data with past climate and palaeoenvironmental conditions. During the warm and wet climate, the lake  
 345 water level is higher. The sediment inflow intensity into the lake's center is significantly reduced and only  
 346 provides low energy transported suspended load of finer fractions deposited as fine silt and clay. Under

347 colder and drier climatic conditions with high energy flow and low lake level, the higher grain size  
348 fractions are transported quickly and deposited in the lake.



349  
350 Fig. 8. Results of end-member modeling (EM1-EM4) using grain size data of Bhimtal lake profile. End-member  
351 represent unmixed grain-size distributions of four end members EM1, EM2, EM3, and EM4. EM1; low energy  
352 conditions, EM2; very shallow lake environment in moderate energy conditions, and EM3 and EM4; fine to coarse  
353 sand fractions during shallow lake-level conditions showing high energy conditions.

354  
355

## 356 8. Conclusion

357

358 The grain-size studies demonstrate that the predominance of sediments is unimodal. The unimodal  
359 distribution palaeolake sediments demonstrate that they were supplied by fluvial action. From the ternary  
360 plot diagram, we can infer that silt predominates, followed by sand and clay. Accumulation of fine silt  
361 indicates a warm climate and high lake level because of substantial monsoon. In contrast, coarse sand  
362 sized particles indicate relatively cold phase and shallow lake level conditions. Except for Zones III, VII,  
363 VIII and IX, the zone-wise distribution of the entire profile indicates that sandy silt concentration is  
364 highest in other zones. Higher concentrations of sandy silt represent high-energy depositional conditions

365 during sediment deposition. It also implies that the catchments have low rainfall or a dry climate with low  
366 lake level. Higher concentrations of silt in Zones III, VII, VIII, and IX indicate low-energy depositional  
367 environments, high lake level and high rainfall in moist climates. The standard deviation results indicate  
368 that the sediment is poorly sorted, concluding that sediment is transported from the proximal source and  
369 deposited under low-energy environmental conditions. The kurtosis value indicates that the samples are  
370 leptokurtic, platykurtic and mesokurtic in nature which indicates changes in the flow characteristics of the  
371 depositional medium. The skewness value of the sediment sample indicates that samples are symmetrical  
372 to very finely skewed, and the variability in the skewness values suggests changes in the hydrodynamic  
373 conditions of the lake. The bivariate plot also suggests that the sediment is mostly finely skewed and  
374 poorly sorted with leptokurtic. The end member analysis suggests that EM1 and EM2 are opposite except  
375 from depths 400-500 cm. The EM3 shows the opposite to EM2 from 0-500 cm and similar trends with  
376 EM1 from depth 500-700 cm. The approach of EEMA provides a means of unraveling sediment fluxes  
377 from catchment areas and other sources, opening the way to significant advances in palaeoclimatic  
378 reconstructions from sediment grain-size distribution data. In general, Bhimtal palaeolake sediments are  
379 generally rich in silt-sized fractions..

380

## 381 **References**

382

- 383 Adrian, R., O'Reilly, C.M., Zagarese, H., Baines, S.B., Hessen, D.O., Keller, W., Livingstone, D.M., Sommaruga,  
384 R., Straile, D., van Donk, E., Weyhenmeyer, G.A., and Winder, M., 2009. Lakes as sentinels of climate change.  
385 *Limnology and Oceanography*, **54**:2283–2297.
- 386 Alin, S.R. and Cohen, A.S., 2003. Lake-level history of Lake Tanganyika, East Africa, for the past 2500 years based  
387 on ostracode-inferred water-depth reconstruction. *Palaeogeography Palaeoclimatology Palaeoecology*, **199**: 31-49.
- 388 Bird, B.W., Polisar, P.J., Lei, Y., Thompson, L.G., Yao, T., Finney, B.P., Bain, D.J., Pompeani, D.P. and Steinman,  
389 B.A., 2014. A Tibetan lake sediment record of Holocene Indian summer monsoon variability. *Earth and Planetary  
390 Science Letters*, **399**: 92-102.
- 391 Blott, S.J and Pye, K., 2001. Gradistat: a grain size distribution and statistics package for the analysis of  
392 unconsolidated sediments. *Earth Surface Processes Landforms*, **26**: 1237–1248.
- 393 Bronk Ramsey, C. 2008. 'Deposition models for chronological records'. *Quaternary Science Reviews*, **27**: 42-60.  
394
- 395 Bronk Ramsey, C., 2009. Bayesian analysis of radiocarbon dates. *Radiocarbon*, **51**: 37–60.  
396
- 397 Bronk Ramsey, C. and Lee, S., 2013. Recent and planned developments of the program OxCal. *Radiocarbon*, **55**:  
398 720–30.  
399
- 400 Chen, J. and Wan, G., 1999. Sediment particle size distribution and its environmental significance in Lake Erhai,  
401 Yunnan Province. *Chinese Journal of Geochemistry*, **18**: 314–320.
- 402 Chen, J.A., Wan, G., Zhang, D.D., Zhang, F. and Huang, R., 2004. Environmental records of lacustrine sediments in  
403 different time scales: sediment grain size as an example. *Science in China Series D: Earth Sciences*, **47**: 954–960.
- 404 Flemming, B.W. 2007. The influence of grain-size analysis methods and sediment mixing on curve shapes and  
405 textural parameters: Implications for sediment trend analysis. *Sedimentary Geology*, **202**, 425-435.



406 Folk, R.L. and Ward, W.C., 1957. Brazos River Bar: a study in the significance of grain size parameters. *Journal of*  
407 *Sedimentary Petrology*, **27**: 3–26.

408 Finney, B. P. and Johnson, T. C., 1991. Sedimentation in Lake Malawi (East Africa) during the past 10,000 years: a  
409 continuous paleoclimatic record from the southern tropic. *Palaeogeography Palaeoclimatology Palaeoecology*, **85**:  
410 351-366.

411 Khanka, L.S. and Jalal, D.S., 1985. Bathymetric analysis of lake Bhimtal, Kumaun Himalaya. In: J.S. Singh  
412 (Editors), *Environmental Regeneration in Himalaya: Concepts and Strategies*. pp.435- 439.  
413

414 Kothiyari, G.C., Kotlia, B.S., Talukdar, R., Pant, C.C., Joshi, M., 2020. Evidences of neotectonic activity along  
415 Goriganga River, higher central Kumaun Himalaya, India. *Geological Journal*, **55(9)**: 6123-6146,  
416 <https://doi.org/10.1002/gj.3791>.

417

418 Kotlia, B.S., 1995. Upper Pleistocene Soricidae and Muridae from Bhimtal-Bilaspur deposits, Kumaun Himalaya,  
419 India. *Journal of Geological Society of India*, **40(6)**:155-171.  
420

421 Kotlia, B. S., 1992. Pliocene murids (Rodentia, Mammalia) from Kashmir basin, northwestern India. *Neues*  
422 *Jahrbuch für Geol. Paläontol. Abhandlungen*, **184**: 339-357.  
423

424 Kotlia, B. S. and Joshi, L. M., 2013. Neotectonic and climatic impressions in the zone of Trans Himadri Fault  
425 (THF), Kumaun Tethys Himalaya, India: A case study from palaeolake deposits. *Zeitschrift für*  
426 *Geomorphologie*, **57**: 289-303.  
427

428 Kotlia, B.S., Kukreti, M., Bisht, H., Singh, A.K., Sharma, A., Kothiyari, G. C., Porinchu, D.F., Chand, P., Kashyap, R.  
429 and Sharma, G.K., 2023. Palaeoenvironmental reconstruction through granulometric analysis of a palaeolake deposit  
430 at Bhikiyasain, Kumaun Lesser Himalaya. *Journal of Climate Change*, **9(1)**: 25-37.  
431

432 Kotlia, B. S. and Rawat, K.S., 2004. Soft sediment deformation structures in the Garbyang palaeolake: evidence for  
433 the past shaking events in the Kumaun Tethys Himalaya. *Current Science*, **87**: 377-379.  
434

435 Kotlia, B. S., Sanwal, J., Phartiyal, B., Joshi, L. M., Trivedi, A. and Sharma C., 2010. Late Quaternary climatic  
436 changes in the eastern Kumaun Himalaya, India, as deduced from multi-proxy studies. *Quaternary International*,  
437 **213 (1-2)**: 44-55.  
438

439 Kotlia, B. S., Schallreuter, I. H., Schallreuter, R. and Schwarz, J., 1998. Evolution of Lamayuru palaeolake in the  
440 Trans Himalaya: palaeoecological implications. *E&G Quaternary Science Journal*, **48(1)**: 177-191.  
441

442 Kotlia, B. S., Sharma, C., Bhalla, M. S., Rajagopalan, G., Subrahmanyam, K., Bhattacharyya, A. and Valdiya, K. S.,  
443 2000. Palaeoclimatic conditions in the Late Pleistocene Wadda Lake, eastern Kumaun Himalaya, India.  
444 *Palaeogeography Palaeoclimatology Palaeoecology*, **162**:105–118.

445 Kotlia, B.S., Shukla, U.K., Bhalla, M.S., Mathur, P.D. and Pant, C.C., 1997. Quaternary vfluvio-lacustrine deposits  
446 of the Lamayuru basin, Ladakh Himalaya: preliminary multidisciplinary investigations. *Geological Magazine*,  
447 **134(6)**: 807-815.  
448

449 Menking, K.M., 1997. Climatic signals in clay mineralogy and grain-size variations in Owens Lake core OL-92,  
450 southeast California. In: Smith, G.I., Bischoff, J.L.(Eds.), *An 800,000 Year paleoclimatic record from core OL-92,*  
451 *Owens Lake, Southeast California, Geological Society of America, Special Paper*, **317**: 37-48.  
452

453 Meyer, I., Davies, G.R., Vogt, C., Kuhlmann, H. and Stuut, J.B.W., 2013. Changing rainfall patterns in NW  
454 Africa since the Younger Dryas. *Aeolian Research*, **10**: 111-123.  
455

456 Padhi, D., Singarasubramanian, S.R., Panda, S. and Venkatesan, S., 2017. Depositional mechanism as revealed  
457 from Grain size measures of Rameswaram coast, Ramanathapuram District, Tamil Nadu, India. *International Journal*  
458 *of Theoretical Applied Sciences*, **9(2)**: 168-177.  
459



- 460 Paterson, G.A. and Heslop, D., 2015. New methods for unmixing sediment grain size data. *Geochemist*  
461 *Geophysics, Geosystems*, **16**: 4494–4506.
- 462  
463 Rawat, V., Rawat, S., Srivastava, P., Negi, P.S., Prakasam, M. and Kotlia, B.S., 2021. Middle Holocene Indian  
464 summer monsoon variability and its impact on cultural changes in the Indian subcontinent. *Quaternary Science*  
465 *Reviews*, **255**:106825..
- 466 Reimer, P.J., Austin, W.E.N., Bard, E., Bayliss, A., Blackwell, P., Bronk Ramsey, C., Butzin, M., Cheng, H.,  
467 Edwards, R.L., Friedrich, M., Grootes, P.M., Guilderson, T.P., Hajdas, I., Heaton, T.J., Hogg, A.G., Hughen, K.A.,  
468 Kromer, B., Manning, S.W., Muscheler, R., Palmer, J.G., Pearson, C., van der Plicht, J., Reimer, R W., Richards,  
469 D.A., Scott, E M., Southon, J.R., Turney, C.S. M., Wacker, L., Adolphi, F., Büntgen, U., Capano, M., Fahrni, S.,  
470 Fogtmann-Schultz, A., Friedrich, R., Kudsk, S., Miyake, F., Olsen, J., Reinig, F., Sakamoto, M., Sookdeo, A., and  
471 Talamo, S., 2020. The IntCal20 Northern Hemispheric radiocarbon calibration curve (0–55 kcal BP). *Radiocarbon*,  
472 **62**: 725–57.
- 473 Sinha, A.K. and Pal, D., 1978. Ecological problems in the high altitude lakes of Nainital area: problems and  
474 suggestions. *Journal of Himalayan Studies*, **2**: 39-43.
- 475  
476 Shuman, B., Bravo, J., Kaye, J., Lynch, J.A., Newby, P. and Webb, T., 2001. Late Quaternary water-level variations  
477 and vegetation history at Crooked Pond, southeastern Massachusetts. *Quaternary Research*, **56**: 401–410.
- 478 Valdiya, K.S., 1988. Geology and Natural Environment of Nainital Hills, Kumaun Himalaya, Nainital, Gyanodaya  
479 Prakashan, pp. 158.
- 480  
481 Valdiya, K.S., Kotlia, B.S., Pant, P.D., Shah, M., Mungali, N., Tewari, S. and Upreti, M., 1996. Quaternary  
482 palaeolakes in Kumaun Lesser Himalaya: finds of neotectonic and palaeoclimatic significance. *Current Science* **70**  
483 **(2)**: 157-161.
- 484  
485 Verkulich, S.R. and Melles, M., 1992. Composition and paleoenvironmental implications of sediments in a fresh  
486 water lake and in marine basins of Bunge Hills, East Antarctica. *Polarforschung*, **60**: 169-180.
- 487 Vriend, M., Prins, M.A., Buylaert, J.P., Vandenberghe, J. and Lu, H., 2011. Contrasting dust supply patterns across  
488 the north-western Chinese Loess Plateau during the last glacial–interglacial cycle. *Quaternary International*, **240**:  
489 167–180.
- 490 Wang, N., Ning, K., Li, Z., Wang, Y., Jia, P. and Ma, L., 2016. Holocene High Lake-levels and Pan-lake Period on  
491 BadainJaran Desert. *Science China Earth Sciences*, **59**: 1633–1641.
- 492 Wang, H., Li, H., Si, J., Zhang, L. and Sun, Z., 2019. Geochemical features of the pseudotachylytes in the Longmen  
493 Shan thrust belt, eastern Tibet. *Quaternary International*, **514**: 173–185.
- 494 Warrier A.K, Shankar R., and Sandeep K., 2013. Sedimentological and carbonate data evidence for lake level  
495 variations during the past 3700 years from a southern Indian lake. *Palaeogeography, Palaeoclimatology,*  
496 *Palaeoecology*.
- 497 Weltje, G.J. and Prins, M.A., 2003. Muddled or mixed? Inferring palaeoclimate from size distributions of deep-sea  
498 clastics. *Sedimentary Geology*, **162**: 39–62.
- 499  
500 Weltje, G.J. and Prins, M.A., 2007. Genetically meaningful decomposition of grain-size distributions. *Sedimentary*  
501 *Geology*, **202(3)**: 409–424.
- 502  
503 Author’s contribution:  
504  
505 The research was conceived by BSK. Field work was carried out by BSK, AKS and LMJ. The sample  
506 analysis was performed by MK, AKS, AS, BP and RK. The manuscript was written by BSK, MK and BP  
507 with input from HB, AS, PC, KG and AM.